

## A Preliminary BeppoSAX Study of the (Bright) Atoll Source GX 9+1

R. Iaria<sup>1</sup>\*, G. Augello<sup>1</sup>, T. Di Salvo<sup>1,2</sup>, N. R. Robba<sup>1</sup>, L. Burderi<sup>3</sup> and L. Stella<sup>3</sup>

<sup>1</sup> Dipartimento di Scienze Fisiche ed Astronomiche, Università di Palermo, Via Archirafi 36, 90123 Palermo, Italy

<sup>2</sup> Astronomical Institute “Anton Pannekoek”, University of Amsterdam and Center for High-Energy Astrophysics, Kruislaan 403, NL 1098 SJ Amsterdam, the Netherlands

<sup>3</sup> Osservatorio Astronomico di Roma, Via Frascati 33, 00040 Monteporzio Catone (Roma), Italy

**Abstract** We report the preliminary results of a 350 ks BeppoSAX observation of the bright atoll source GX 9 + 1. In the field of view of the MECS instrument we discovered a X-ray pulsar, designated SAX J1802.7–2017, at an angular distance from GX 9+1 of  $\sim 22'$ . Since the X-ray emission of SAX J1802.7–2017 contaminates the energy spectrum above 10 keV we studied the energy spectrum of GX 9 + 1 in the energy band 0.1–10 keV. We selected four regions in the color-color diagram and extracted one spectrum from each region. A bump below 1 keV is present in the spectra using a model composed by a Comptonized component absorbed by neutral matter having an equivalent hydrogen column of  $1.5 \times 10^{22} \text{ cm}^{-2}$ . The bump disappears adding an overabundance of iron and nickel of 7 and 70 with respect to the solar iron abundance and to the solar nickel abundance, moreover the equivalent hydrogen column becomes  $0.5 \times 10^{22} \text{ cm}^{-2}$  suggesting a possible distance to the source of 4.5 kpc, implying a luminosity of  $4 \times 10^{37} \text{ erg s}^{-1}$  and that the bright atoll source GX 9 + 1 is not bright but it is a typical atoll source.

**Key words:** accretion discs – stars: individual: GX 9+1 — stars: neutron stars — X-ray: stars — X-ray: spectrum — X-ray: general

### 1 INTRODUCTION

The first observation of GX 9+1 (4U 1758–205) was taken in 1966 using a proportional counter sensible in the 1.5–10 keV energy band on board of a missile (Gursky et al. 1967). Two years later the presence of the source was confirmed by Bradt et al. 1968 which also identified the position of the source at a Galactic longitude of  $9.1^\circ$  and a Galactic latitude of  $1.2^\circ$ , collocating the source in the Galactic bulge. Until now the distance and the companion star of GX 9+1 are unknown. Langmeier et al. 1985, using the Medium Energy (ME) instrument on board of EXOSAT, performed a spectral and timing analysis of an observation of GX9+1 in the

---

\* E-mail: [iaria@gifco.fisica.unipa.it](mailto:iaria@gifco.fisica.unipa.it)

energy band 1–30 keV. During the observation, the source flux varied irregularly in time scales from minutes to hours. No periodic emission in the period range from 16 msec to 2000 s was found with an upper limit of around 1 percent ( $3\sigma$ ) for the pulsed fraction. The hardness ratio ( $[3.4 - 7.5 \text{ keV}] / [1 - 3.2 \text{ keV}]$ ) showed a correlated change with the flux intensity indicating that the source belongs to the class of Low-Mass X-ray Binaries (LMXBs). The energy spectrum was fitted by a double component model, a black body component ( $kT = 1.16 - 1.26 \text{ keV}$ ), probably produced in a region near the neutron star surface, together with a thermal bremsstrahlung law ( $kT = 13 - 15 \text{ keV}$ ) probably connected to phenomena due to a presence of an accretion disk. No iron line was detected. White et al. (1988) reanalysed the ME EXOSAT energy spectrum fitting the data with a blackbody component, with a temperature of 1.5 keV, plus a Comptonized component having an electron temperature of 3 keV, both these components were absorbed by neutral matter having an equivalent hydrogen column of  $2.1 \times 10^{22} \text{ cm}^{-2}$ . The extrapolated luminosities, in the 0.1–30 keV, associated to the blackbody and to the Comptonized component were  $6 \times 10^{37} \text{ erg s}^{-1}$  and  $1.7 \times 10^{38} \text{ erg s}^{-1}$  respectively, assuming an arbitrary distance to the source of 10 kpc. The distance of 10 kpc was probably assumed because the source is in the direction of the Galactic center anyway, since that work, the idea that the source was a high luminous X-ray source was associated to GX 9+1. Hasinger & van der klis (1989), studying the fast timing properties of GX 9+1 with EXOSAT data, conclude that the source is to be included in the low intensity atoll class, then it should have a luminosity between  $10^{36} \text{ erg s}^{-1}$  and  $10^{37} \text{ erg s}^{-1}$ , typical of the LMXBs belonging to the atoll class. However, since its high luminosity previously estimated, GX 9+1 was defined as a bright atoll source.

## 2 OBSERVATIONS

The observation of the GX 9+1 field was carried out from 2001 September 16 02:01:30.0 (UTC) to 2001 September 20 03:00:08.5 (UTC), using the co-aligned Narrow Field Instruments (NFIs) on board BeppoSAX. These are: a Low Energy Concentrator Spectrometer (LECS; energy range 0.1–10 keV; Parmar et al. 1997, two Medium Energy Concentrator Spectrometers (MECS; energy range 1–10 keV; Boella et al. 1997), a High Pressure Gas Scintillation Proportional Counter (HPGSPC; energy range 7–60 keV; Manzo et al. 1997), and a Phoswich Detector System (PDS; energy range 13–200 keV; Frontera et al. 1997). The exposure times were  $\sim 60 \text{ ks}$ ,  $\sim 149 \text{ ks}$ ,  $\sim 142 \text{ ks}$ ,  $\sim 71 \text{ ks}$ , for LECS, MECS, HPGSPC and PDS, respectively. The circular fields of view (FOV) of the LECS and MECS are  $37'$  and  $56'$  in diameter respectively, while those of the HPGSPC and PDS are hexagonal with FWHM of  $78'$  and  $66'$ , respectively. The LECS and MECS detectors are position sensitive counters with imaging capability. The position reconstruction uncertainty for MECS is  $0.5'$  in the central area of  $9'$  radius, and  $\sim 1.5'$  in the outer region of the FOV (Boella et al. 1997). The HPGSPC and PDS systems do not have imaging capabilities, and their data are therefore difficult to interpret and analyse for individual sources when the FOV includes more than one source. A fainter source, designated SAX J1802.7–2017, is visible in the MECS FOV at R.A.(2000.0) =  $18^{\text{h}}02^{\text{m}}39.9^{\text{s}}$  and Dec.(2000.0) =  $-20^{\circ} 17' 13.50''$  (position uncertainty  $2'$ ), at an angular distance from GX 9+1 of  $\sim 22'$  (Augello et al. 2003). We can be sure that the source was within the PDS FOV, because the source X-ray pulsations were detected also in the PDS data (see figure 6 in Augello et al. 2003). In Fig. 1 we report on the SAX J1802.7–2017 lightcurve in the 1–10 keV energy range and the background count rate of our observation in the 1–10 keV energy range (see also Augello et al. 2003). During the first 50 ks the source count rate is overwhelmed by the background emission (gray interval in Fig. 1) while it reaches the maximum from 50 ks up to 140 ks from the beginning of the observation (pink interval in Fig. 1).

In Fig. 2 we plotted the lightcurve of GX 9+1 in the energy band 1–10 keV. The count rate is highly variable during the entire observation ranging from  $\sim 120 \text{ counts s}^{-1}$  up to  $\sim$

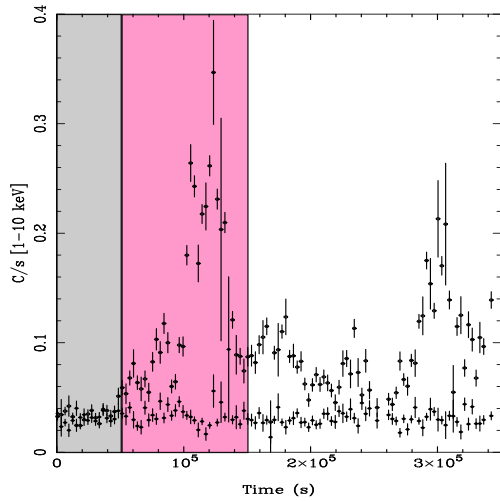


**Fig. 1** Lightcurves of SAX J1802.7–2017 and of the background. The bin time is 3000 s. During the first 50 ks (gray interval) the X-ray pulsar has its count rate comparable to the background one. From 50 ks to 140 ks (pink interval) SAX J1802.7–2017 reaches the maximum count rate.

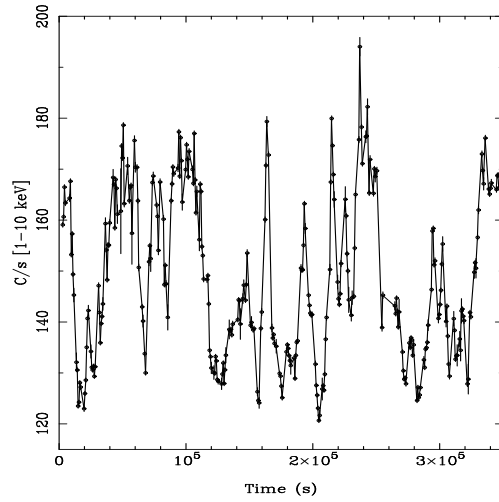


**Fig. 2** GX 9+1 lightcurve in the energy band 1–10 keV (MECS data). The open circles are the GX 9+1 count rate; to sake of clarity we interpolated them. The bin time is 697 s.

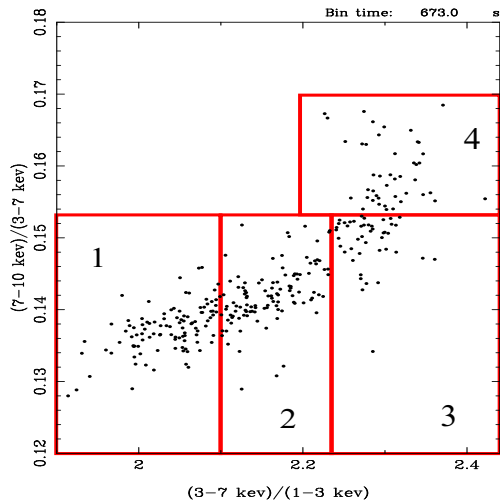


**Fig. 3** Color-color diagram of GX 9+1. The bin time is 673 s. The boxes indicate the four zones selected from which we extracted the corresponding energy spectra.

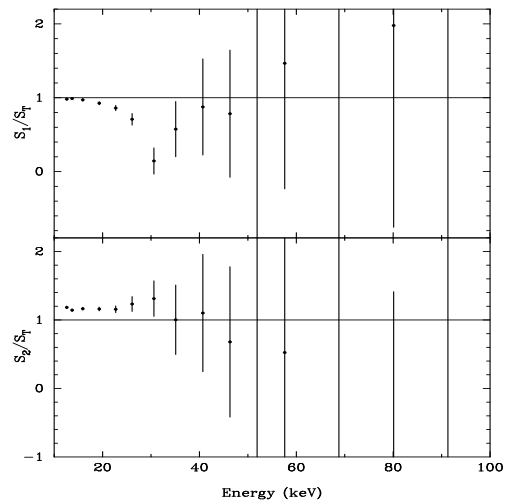


**Fig. 4** Upper panel: ratio between the PDS spectrum  $S_1$  (see text) with respect to the PDS spectrum  $S_T$  (see text). Lower Panel: ratio between the PDS spectrum  $S_2$  (see text) with respect to  $S_T$ .

**Table 1** In Cols. 2 and 3 we report on the intervals of Soft Color (SC) and Hard Color (HC) which identify the four zones selected on the color-color diagram. In the others columns the exposure time, in ks, of LECS and MECS instruments is reported.

| Zone | SC<br>interval | HC<br>interval | LECS<br>ks | MECS<br>ks |
|------|----------------|----------------|------------|------------|
| 1    | 1.9–2.1        | 0.12–0.153     | 21         | 54         |
| 2    | 2.1–2.24       | 0.12–0.153     | 22         | 51         |
| 3    | 2.24–2.44      | 0.12–0.153     | 7          | 17         |
| 4    | 2.2–2.44       | 0.153–0.17     | 6          | 21         |

200 counts  $s^{-1}$ . In Fig. 3 we plotted the color-color diagram (CD), where the hard color (HC) is the ratio between the count rate in the energy band 7–10 keV to that in the energy band 3–7 keV and the soft color (SC) is the ratio between the count rate in the 3–7 keV energy band to the count rate in the 1–3 keV energy band. Since the high variability of GX 9+1 we selected four zones on the CD (see Fig. 3) and extracted the corresponding energy spectra from them. In Table 1 we report the intervals of SC and HC which identify the four selected zones, furthermore the exposure time of LECS and MECS data is also reported.

Since the X-ray pulsar SAX J1802.7–2017 is far to GX 9+1  $\sim 22'$ , it is present in the HP and PDS FOV and since the HP and PDS instruments have not image capability we have to check a possible contamination of SAX J1802.7–2017 in these data. To verify this we computed:

1. the ratio between the PDS spectrum during the first 50 ks ( $S_1$ ), when the SAX J1802.7–2017 count rate is comparable to the background count rate, and the PDS spectrum of the entire observation,  $S_T$ .
2. the ratio between the PDS spectrum during the large flare of SAX J1802.7–2017 ( $S_2$ ), corresponding to the pink interval in Fig. 1, and  $S_T$ .

We added to both the spectra a systematic error of 1%. In the energy range 10–40 keV the ratio is less than 1 and greater than 1 respectively when the X-ray pulsar count rate is low and during the maximum activity of the X-ray pulsar (see Fig. 4, upper and lower panel). These results could be affected by the presence of SAX J1802.7–2017 in the PDS FOV and/or by an intrinsic variation of the hard spectrum of GX 9+1, however the temporal intervals used to extract the spectra  $S_1$  and  $S_2$  seem to indicate that the main cause of the spectral variation is the presence of the X-ray pulsar. These results constrain us to analyze only the LECS and MECS data for the study of GX 9+1.

### 3 SPECTRAL ANALYSIS AND PRELIMINARY DISCUSSION

We extracted the energy spectra for LECS and MECS as reported by Iaria et al. (2004) and a systematic error of 1% was added to the data. The energy ranges used for the spectral analysis are 0.12–3.7 keV for the LECS and 2.2–10 keV for the MECS. We will named the four spectra from 1 to 4 correspondingly to the four selected zones on the CD.

We fitted the continuum emission between 0.1 and 10 keV using a Comptonization model (*Comptt* in XSPEC, Titarchuk 1994) absorbed by neutral matter. This model gave a  $\chi^2/d.o.f.$  of 297/157, 289/157, 211/157 and 196/157, respectively from the spectrum 1 to the spectrum 4. The equivalent absorption hydrogen column was  $\sim 1.5 \times 10^{22} \text{ cm}^{-2}$ , the seed-photon temperature and the electron temperature of the Comptonized component around 0.5 keV and 2 keV respectively, and finally the optical depth,  $\tau$ , of the Comptonizing cloud 20. The residuals with respect to this model are shown in Fig. 5.

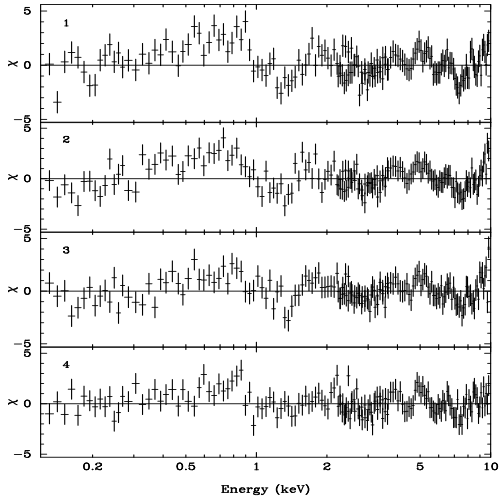


**Fig. 5** Residuals in units of  $\sigma$  for the spectra 1, 2, 3 and 4 from the top to the bottom respectively. The residuals are with respect to the model composed by a Comptonized component absorbed by an equivalent hydrogen column of  $1.5 \times 10^{22} \text{ cm}^{-2}$ .

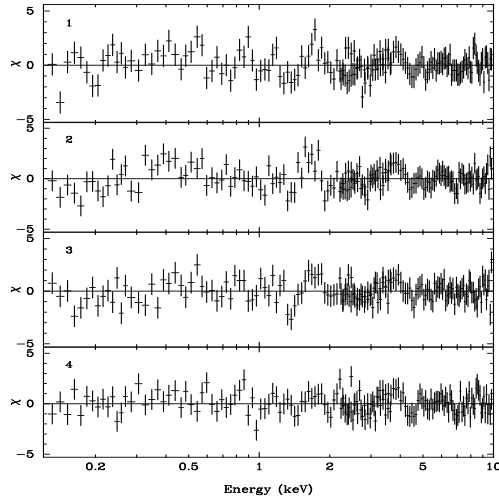


**Fig. 6** Residuals in units of  $\sigma$  for the spectra 1, 2, 3 and 4 from the top to the bottom respectively. The residuals are with respect to the model composed by a Comptonized component, absorbed by an equivalent hydrogen column of  $\sim 0.5 \times 10^{22} \text{ cm}^{-2}$  and with an overabundance of iron and nickel with respect to the solar abundance.

The residuals show a soft excess below 1 keV which is more evident in the spectra 1 and 2 probably because the exposure time of the LECS is larger (see Table 1). The excess has the same behaviour for each spectrum, reaching the maximum at 0.6–0.7 keV. We tried several emission components to fit the soft excess but no one gave reasonable results. The addition of a further blackbody component with a temperature of  $\sim 0.05 \text{ keV}$  gave a corresponding luminosity of  $\sim 10^{40} \text{ erg s}^{-1}$  in the 0.1–200 keV energy range assuming a distance to the source of 8 kpc. This result is very hard to explain assuming that the X-ray binary system contains a neutron star. Instead of a blackbody we added a Gaussian line centered at 0.6 keV, also in this case the results were not physically clear because the corresponding equivalent width of the line was larger than 3 keV. The value of the equivalent hydrogen column should imply that the emission below 1 keV is absorbed by the neutral matter while we find a soft excess at those energies. There are two possible explanations of this:

1. There is a continuum emission component below 1 keV absorbed by a lower equivalent hydrogen column.
2. The equivalent hydrogen column of the whole spectrum is overestimated.

We exclude the first hypothesis; in fact, the residual below 1 keV disappears adding in the spectra 1, and 2 a continuum emission component absorbed by a lower value of equivalent hydrogen column ( $N_{\text{H}} \sim 4 \times 10^{20} \text{ cm}^{-2}$ ) than that absorbing the Comptonized component ( $\sim 1.5 \times 10^{22} \text{ cm}^{-2}$ ). However in this case it is hard to explain the lower value of  $N_{\text{H}}$  since the emitting source should be distant less than 1 kpc. On the other hand in the spectra 3 and 4, where the residual below 1 keV is less prominent, the equivalent hydrogen column absorbing the new component increases more than one order of magnitude up to  $\sim 1.5 \times 10^{22} \text{ cm}^{-2}$  and

this cannot explain the possible scenario described above except that assuming a not realistic increase of more than one order of magnitude of the neutral matter around the binary system. For these reasons we conclude that the second hypothesis is more reasonable. A good fit was obtained using a model of photoelectric absorption with an overabundance of iron and nickel with respect to the solar abundance listed by Anders & Grevesse (1989) (*vphabs* in XSPEC). The continuum is described by a Comptonized component also in this case and its parameters do not change with respect to the initial model. The equivalent hydrogen column is  $N_{\text{H}} \sim 5 \times 10^{21} \text{ cm}^{-2}$ . The abundance of iron is a factor 7 larger than the solar iron abundance and the abundance of nickel is a factor 70 larger the solar nickel abundance. The overabundance of iron and nickel well fit the energy spectrum in the whole energy band 0.1–10 keV because the component *vphabs* adds deeper L-shell absorption edges of these two elements at around 1 keV. In the initial model the fit is driven by the energy spectrum above 1 keV since the high statistics of the source at those energies, then the software minimizes the fit using an equivalent hydrogen column of  $\sim 1.5 \times 10^{22} \text{ cm}^{-2}$  that underestimates the emission below 1 keV giving as result the presence of a bump at these energies. The addition of an overabundance of iron and nickel is more statistically significant in the spectra 1 and 2 where the LECS exposure time is larger (see Table 1). An absorption edge at 5.5 keV was also added to the model. This could correspond to the edge of Ca XX. This model gave a  $\chi^2/d.o.f.$  of 180/153, 183/153, 152/153 and 150/153, respectively from the spectrum 1 to the spectrum 4 and the probability of chance improvement for the addition of the Fe overabundance, Ni overabundance and the Ca xx absorption edge is  $\sim 0$  for each spectrum. The residuals of this model are plotted in Fig. 6.

Further investigations have to be done about the overabundance of iron and nickel, however from this preliminary result one point is put on light: the value of  $N_{\text{H}} \sim 5 \times 10^{21} \text{ cm}^{-2}$  should indicate that GX 9+1 is distant 4.5 kpc, while until now a distance to GX 9+1 of 10 kpc was supposed (White et al. 1988). The estimated unabsorbed luminosity in the energy band 0.1 – 200 keV is  $\sim 4 \times 10^{37} \text{ erg s}^{-1}$ , a typical value for an atoll source. Then the bright atoll source GX 9+1 could not be so bright.

**Acknowledgements** This work was partially supported by the Italian Space Agency (ASI) and the Ministero della Istruzione, della Università e della Ricerca (MIUR).

## References

- Anders E., Grevesse N., 1989, *Geochimica et Cosmochimica Acta*, 53, 197  
 Augello G., Iaria R., Robba N. R. et al., 2003, *ApJ*, 596, L63  
 Boella G., Butler R. C., Perola G. C., et al. 1997, *A&AS*, 122, 299  
 Bradt H., Naranan S., Rappaport S. et al., 1968, *ApJ*, 152, 1005  
 Frontera F., Costa E., dal Fiume D. et al., 1997, *A&AS*, 122, 357  
 Gursky H., Gorenstein P., Giacconi R., 1967, *ApJ*, 150, 75  
 Hasinger G., van der Klis M., 1989, *A&A*, 225, 79  
 Iaria R., Di Salvo T., Robba N. R. et al., 2004, *ApJ*, 600, 358  
 Langmeier A., Sztajno M., Trumper J. et al. 1985, *SSRv*, 40,367  
 Manzo G., Giarrusso S., Santangelo A. et al., 1997, *A&AS*, 122, 341  
 Parmar A. N., Martin D. D. E., Bavdaz M. et al., 1997, *A&AS*, 122, 309  
 Titarchuk L., 1994, *ApJ*, 434, 570  
 White N. E., Stella L., Parmar A. N., 1988, *ApJ*, 324, 363